Real-Time Label-Free Direct Electronic Monitoring of Topoisomerase Enzyme Binding Kinetics on Graphene

Laura Zuccaro,[†,‡] Cinzia Tesauro,[‡,§] Tetiana Kurkina,[†] Paola Fiorani,[‡,∥] Hak Ki Yu,[⊥] Birgitta R. Knudsen,[§,#] Klaus Kern,[†,▽] Alessandro Desideri,[‡] and Kannan Balasubramanian*[,†]

[†]Max Planck Institute for Solid State Research, D-70569 Stuttgat, Germany, [‡]Department of Biology, University of Rome Tor Vergata, I-00133 Rome, Italy, [§]Department of Molecular Biology & Genetics, Aarhus University, DK-8000 Aarhus, Denmark, [∥]Institute of Translational Pharmacology, National Research Council CNR, I-00133 Rome, Italy, [⊥]Max Planck Institute for Biophysical Chemistry, 37077 Göttingen, Germany, [#]Interdisciplinary Nanoscience Center (iNANO), Aarhus University, DK-8000 Aarhus, Denmark, and [▽]Institut de Physique de la Matière Condensée, École Polytechnique Fédérale de Lausanne, CH-1015 Lausanne, Switzerland

ABSTRACT Monolayer graphene field-effect sensors operating in liquid have been widely deployed for detecting a range of analyte species often under equilibrium conditions. Here we report on the real-time detection of the binding kinetics of the essential human enzyme, topoisomerase I interacting with substrate molecules (DNA probes) that are immobilized electrochemically on to monolayer graphene strips. By monitoring the field-effect characteristics of the graphene biosensor in real-time during the enzyme–substrate interactions, we are able to decipher the surface binding constant for the cleavage reaction step of topoisomerase I activity in a label-free manner. Moreover, an appropriate design of the capture probes allows us to distinctly follow the cleavage step of topoisomerase I functioning in real-time down to picomolar concentrations. The presented results are promising for future rapid screening of drugs that are being evaluated for regulating enzyme activity.

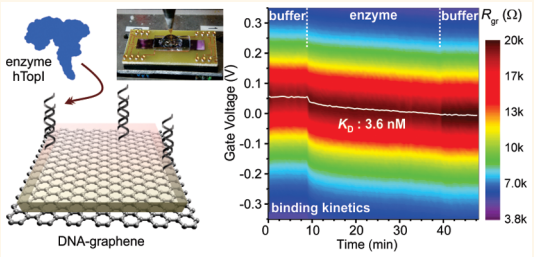

KEYWORDS: label-free biosensing · human topoisomerase · enzyme activity · biosensor · field effect

Nanoscale devices made of single nanostructures (such as monolayer graphene) are emerging as promising candidates for the next generation of biosensors.[1,2] Since every atom in the sp^2-bonded honeycomb lattice of graphene is a surface atom, it exhibits a very high surface-to-volume ratio, thereby showing promise for ultimate sensitivity.[3] In order to obtain reactivity with a particular target analyte, the graphene surface is chemically modified with appropriate receptor molecules that can bind the analyte.[4,5] A number of chemical functionalization strategies have been reported, of which electrochemical modification has specific advantages such as the selective attachment of receptors on to contacted graphene flakes,[6] good control over the density of functionalities,[7] and the capability to tune the isoelectric point of the graphene–liquid interface.[8] Moreover, the detection is label-free, and the binding of the analyte on to immobilized receptors can be directly deciphered by monitoring the electrical characteristics, such as the field-effect response.[1] This avoids the need for any secondary reactions after binding or sandwich protocols keeping the entire detection scheme simple, while preserving the high sensitivity inherent in such a sensing architecture. Using monolayer graphene field-effect devices, a number of examples have been demonstrated for the detection of nucleic acids, proteins, peptides, and metabolites with very high sensitivity and low detection limits.[9−14] Typically, the detection is done under equilibrium or steady-state conditions, *i.e.*, measuring the sensor response before and after the binding event. Here, we perform the detection in real-time by continuously monitoring the field-effect characteristics, enabling us to obtain information about the kinetic aspects of the binding interactions. In this manner, we extract the surface binding constant of enzyme molecules interacting with their substrate immobilized on graphene. Many other transduction principles have been utilized for binding

* Address correspondence to b.kannan@fkf.mpg.de.

Received for review July 28, 2015 and accepted October 7, 2015.

Published online October 07, 2015
10.1021/acsnano.5b05709

kinetics such as surface plasmon resonance (SPR),[15,16] high-Q microcavities,[17] and nanomechanical resonators.[18] In contrast to these techniques electronic label-free biosensing allows for a simpler signal readout minimizing the need for complex instrumentation, which will allow for a comparatively easier integration with smartphones or tablets. Moreover, direct label-free electronic detection has demonstrated detection limits down to the attomolar range.[19]

Using silicon- or graphene-based electrical devices, the detection of binding kinetics has been often reported,[20−24] however, there is no demonstration yet of the direct label-free electronic observation of catalytic activity of an (electrochemically inactive) enzyme aliquot. There is one example of detecting enzyme−substrate interactions using a silicon ribbon device.[25] However, in this case, the silicon nanosensor functions mainly as a pH sensor, which detects changes in pH after the enzyme reaction takes place in solution. There is also a series of experiments performed by one group to electronically monitor the activity of single enzyme molecules fixed onto individual carbon nanotubes.[26−28] However, in this case, the substrate molecules were present in the micromolar range, and data were collected over a long time in order to extract the required information by an elaborate statistical analysis. In contrast to all these experiments, where the enzyme is the receptor immobilized on the sensor surface, in our case the enzyme is the analyte that we would like to detect, while the substrate is the receptor that is immobilized on the nanostructure surface. Using such a strategy, it is straightforward to deploy the sensor for a realistic application where the amount of enzyme present in a crude sample is unknown. Moreover, in this configuration it is possible to follow the enzyme−substrate interactions at picomolar enzyme concentrations thereby providing an added merit of higher sensitivity.

In order to demonstrate the capability of real-time label-free direct electronic monitoring on graphene, we have chosen to follow the activity of the enzyme human DNA topoisomerase IB (hTop1). hTop1 relaxes DNA topological stress associated with vital cellular processes such as replication or transcription, in order to preserve the genome stability and maintain its topological state.[29,30] hTop1 catalyzes the relaxation of supercoiled DNA by clamping on to the DNA helix,[31] making a nick (called the cleavage reaction step), relaxing the stress by strand rotation, and rejoining the relaxed DNA by ligation (religation reaction step), followed by enzyme release.[32] The clamping of the enzyme to the helix is noncovalent, while the cleavage reaction involves a nucleophilic attack by a tyrosine residue on one DNA strand, resulting in the formation of a transient covalent hTop1-DNA complex.[32] Topoisomerases are an interesting class of enzymes since they are the targets of numerous inhibitors that are evaluated as anticancer drugs.[33] These small molecules act by stabilizing the hTop1-DNA complex, reducing the probability for subsequent steps, eventually leading to DNA damage and cell death.[34] This motivates our realization of an electronic label-free graphene biosensing platform for detection of hTop1 activity, which will be extremely useful in the future for rapid screening of the efficacy of anticancer drugs. On the other hand, the binding kinetics will provide us insight into the mechanisms of both the ability and resistance of a selected drug to inhibit hTop1 activity.[35−37]

Many protocols have been developed to assay the activity of hTop1,[38,39] the most common of them being the "relaxation assay", which assesses the catalytic activity as a whole by comparing the proportion of supercoiled and relaxed DNA. In order to distinguish the cleavage and religation steps of hTopI activity, cleavage assays have been developed, where an appropriately designed DNA molecule (referred to as *Topo Suicide*) is used as a capture probe to bind to the enzyme.[40,41] Steady-state response of such binding interactions could be detected by using radio labels[40] or fluorescent quantum dots.[42] Recently by using a labeled rolling circle amplification assay, we have demonstrated a detection limit down to the picomolar range.[43] In addition to steady-state measurements, the ability to measure the kinetics of such binding interactions is expected to provide us with an improved understanding of the mechanism of drug action and drug resistance.[44] Recently, a Förster resonance energy transfer (FRET)-based DNA sensor has been demonstrated enabling the real-time observation of enzyme activity in high nanomolar concentrations[45] that allowed for the identification of the mechanism of catalytic action in hTop1.[46] All of these assays require some kind of labeling or secondary reaction steps and hence are expensive, time demanding, or are not easily amenable for field-use and rapid screening. In contrast to these assays, the presented strategy does not require labeling of the enzymes or the substrates using markers such as dyes, fluorophores, radioisotopes, nanoparticles, beads, *etc*. and is hence a label-free technique. Label-free surface plasmon resonance (SPR)-based methods have been deployed to directly study the interaction of plasmid DNA with enzymes, however in these cases the enzymes were immobilized, and the DNA was the analyte.[47,48] There are a few examples with immobilized capture DNA probes used to analyze the binding of hTop1, however the detection limit is in the high nanomolar range.[49,50] Moreover, in none of the above studies, it has been possible to observe the cleavage and religation steps distinctly in real-time, especially at subnanomolar concentrations.

RESULTS/DISCUSSION

Monolayer graphene devices were fabricated on Si/SiO_2 chips using chemical vapor deposition (CVD)-grown

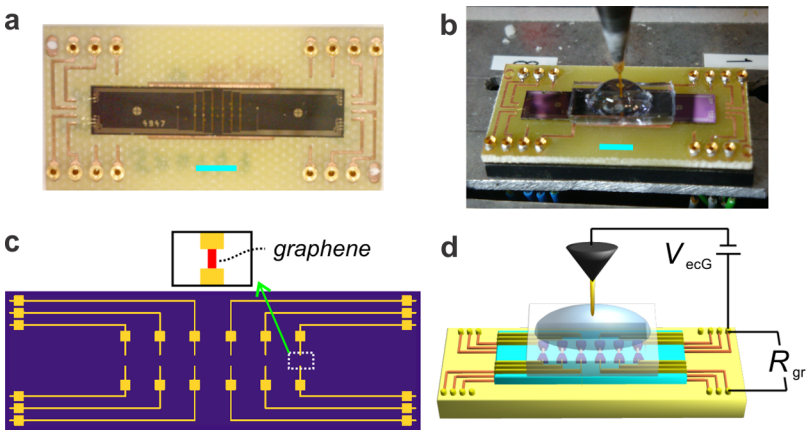

Figure 1. Photos and layout of the sensor chip. (a,b) Photos of the sensor chip in the dry state (a) and in liquid during a sensor trial (b). (c,d) Layout of the sensor chip in the dry state (c) and in liquid (d). The liquid is brought in contact with the sensor chip using a PDMS well. Each chip is equipped with six electrode pairs that incorporate a gap, where the graphene strip (red stripe in (c)) is patterned. The resistance across one of the graphene strips (R_{gr}) is measured continuously as a function of the voltage applied to the gate electrode (V_{ecG}; ecG: electrochemical gate). A Ag/AgCl reference electrode serves as the gate electrode. Scale bars in (a) and (b): 5 mm.

graphene obtained commercially or using a peel-off strategy.[51] Details of the fabrication procedure are presented in the Methods section.[8] At the end of the fabrication process we are left with a graphene strip of size around 2 × 2 μm contacted by electrodes. The liquid is brought in contact with the graphene surface with the help of a microchannel cast out of poly-(dimethylsiloxane) (PDMS). We ensure that the graphene strip is exclusively in contact with the solution by passivating all electrode lines using silicon oxide. The device layout and photos of a sensor chip are shown in Figure 1. The electronic measurements are carried out by measuring the real part of the impedance (or the resistance) of the device at a frequency of around 1 kHz continuously. The field-effect configuration is realized by using a Ag/AgCl reference electrode as the gate electrode. Here, the resistance of the graphene strip (R_{gr}) is measured as a function of the electrochemical gate voltage (V_{ecG}) applied to the reference electrode. The principle behind the working of such field-effect sensors is based on changes in the electrostatic charge distribution that occur at the graphene–liquid interface, when the analyte molecules bind to the sensor surface.[1,20] These changes in charge distribution are detected as voltage shifts in the measured field-effect characteristics. Hence, by continuously monitoring the device resistance as a function of the gate voltage, we are able to follow the kinetics of the binding of analyte molecules on to the sensor surface.[21]

Purified aliquots of the enzyme hTop1 were prepared from yeast cells transformed with a plasmid containing the hTop1 gene as discussed in the Methods section.[43] The sensing protocol for the detection of hTop1 is shown in the scheme in Figure 2a–c. To detect the activity of hTop1, the graphene surface should be provided with selected DNA capture probes, which are substrates for hTop1 catalysis. We perform the attachment of DNA in two steps as we have done earlier on carbon nanotubes: first, the graphene surface is enriched with carboxyl groups through electrochemical modification,[8,52] while in the second step amine-terminated DNA receptors are coupled to the carboxyl groups through carbodiimide coupling (see Figure S1 and SI for details).[19] In order to monitor the activity of hTop1, we decouple the two major reaction steps through an appropriate design of the DNA sequence (Figure 2d–f). The reason for this decoupling is two-fold. First the kinetics of binding interactions is expected to be different during the two reaction steps.[32] Second, this decoupling is necessary, in order to exploit the full capability of label-free real-time detection for future applications in drug screening. The drugs targeting hTop1 can be classified under two categories: class I drugs (also called catalytic inhibitors) that interfere with the hTop1-DNA complex formed during the cleavage step, and class II drugs (referred to as poisons) that have an effect on the religation step.[44,53] The ability to distinguish the two steps of the reaction will allow for an unambiguous understanding of the mechanism of drug action. The capture probes in Figure 2d–f are designed with this goal in mind, wherein the DNA sequence (GACTT*AG, representing a highly preferred interaction site for hTop1)[54] is inserted into a partially duplex DNA, with a single stranded extension downstream the binding site (red sequence in Figure 2d–f). In such a situation, the enzyme is able to bind and cleave the DNA (at the location of the arrow), however the religation step is prevented because the generated dinucleotide downstream of the binding site diffuses away from the complex.[40,41] Due to the absence of a free hydroxyl group, hTop1 remains covalently bound to the 3′-end of the DNA receptor substrate. This religation step can however be triggered by addition of molar excess

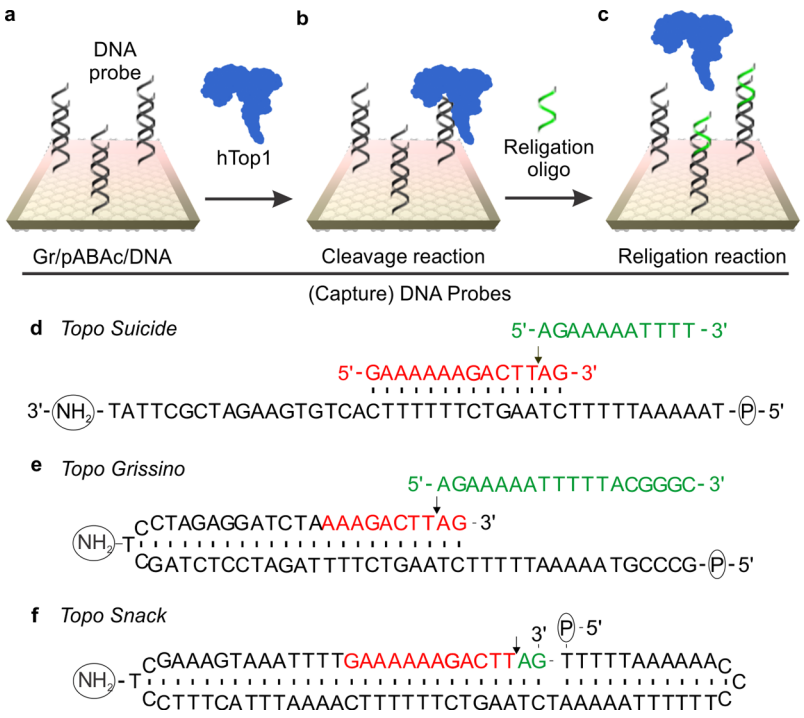

Figure 2. Schematic of the sensing strategy. (a) The sensors deployed here contain as the active element monolayer graphene strips that are functionalized with capture DNA probes (see SI for details on DNA coupling). The DNA probes are designed in such a way that the two major reaction steps of hTop1 activity (cleavage (b) and religation (c) steps) can be decoupled. (b) When the DNA-functionalized graphene is exposed to hTop1, the enzyme binds and cleaves the DNA strand forming a transient covalent complex with the DNA (cleavage reaction). (c) Upon addition of an appropriate religation oligonucleotide, hTop1 uses the free 5′-OH to ligate the added single strand (religation reaction) with or without release of the enzyme. (d–f) Sequences of three different capture DNA probes used in this study: *Topo Suicide*, *Topo Grissino*, *Topo Snack*. The amine termination is used to couple to the activated COOH groups on functionalized graphene. In red are sequences containing the preferred recognition site specific for hTop1 (scissile strand), while the black region indicates the nonscissile strand. The cleavage site is indicated by an arrow. In green are the religation oligonucleotides. The 5′-phosphate is required to avoid nonspecific religation.

of an oligonucleotide that is complementary to the single-stranded extension (the green sequences in Figure 2d–f).[39,55] As shown in the scheme of Figure 2, in a first series of measurements we focus exclusively on the cleavage step by monitoring the electrical characteristics of the DNA-functionalized graphene device in the presence of hTop1. In a second set of experiments, we have monitored the religation step additionally by adding the religation oligonucleotide to the enzyme-bound graphene device.

First we present a typical kinetic response of the binding of hTop1 on to DNA-functionalized graphene. For this purpose, we sweep the electrochemical gate voltage (V_{ecG}) in a certain voltage range and measure the resistance (R_{gr}) of the device continuously over time resulting in a 2D map ($R_{gr}(V_{ecG}, t)$)[8] of the evolution of the sensor response, where t denotes the start time of a gate sweep cycle. The time for every cycle is set by the speed of gate sweep, which is around 30 mV/s here. Such a 2D map in the absence of hTop1 is shown in Figure 3a for the DNA-functionalized graphene device in reaction buffer (RB) containing 20 mM Tris/HCl, 0.1 mM Na_2EDTA, 10 mM $MgCl_2$, and 50 mM KCl (pH 7.5). The components of this buffer are chosen in order to maintain the proper functioning of the enzyme.[43]

Apart from a small drift at the beginning of the measurement, the field-effect response remains rather constant for a time period of around 30 min. Figure 3b shows the response of the same device upon introduction of 300 pM (final concentration) of hTop1 into the microchannel. The response is measured for around 30 min, and the solution is copiously exchanged with the initial RB. From the gate dependence of resistance measured at every cycle we extract the Dirac point (as the gate voltage of resistance maximum) and plot this as a function of time in Figure 3c. It is apparent that in the absence of the enzyme, the Dirac point remains constant, while in the presence of hTop1, a clear shift in the Dirac point toward negative gate voltages is observed. This is further confirmed by the steady-state response in Figure 3d, where the transfer curves in RB with and without hTop1 are shown. A shift of the Dirac point toward negative gate voltages occurs when there is additional positive charge introduced during the binding.[8,56] Here, this additional positive charge can be correlated with the charge due to the bound enzyme (isoelectric point 9.3) molecules which are positively charged at our working pH of 7.5. It is worth mentioning that we are sensitive to biomolecular interactions at the graphene–liquid interface in spite

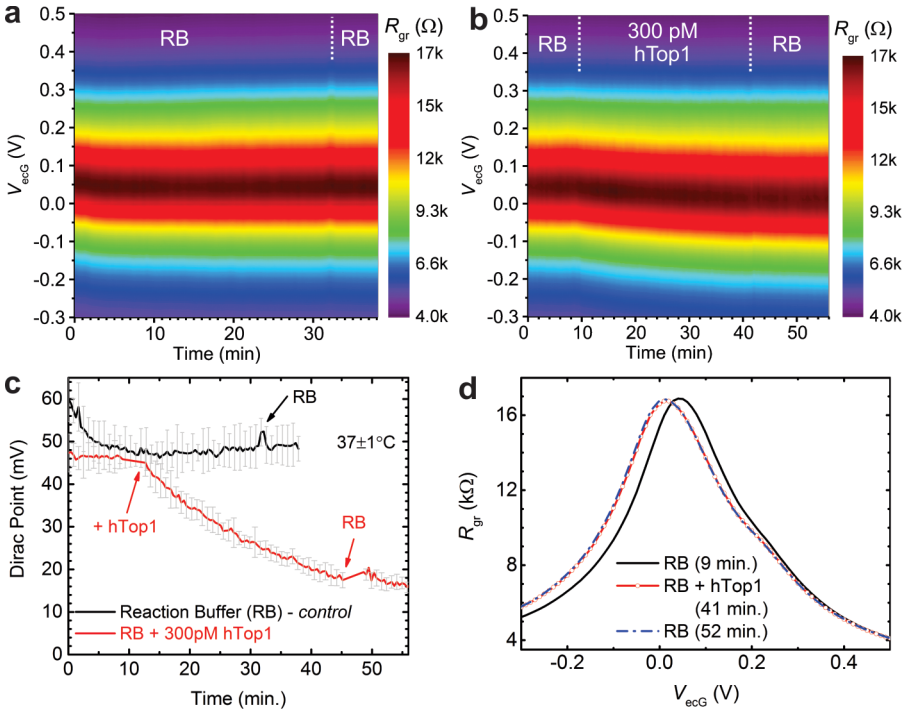

Figure 3. Real-time detection of hTop1 cleavage reaction. (a,b) Real-time sensor response of a capture-DNA (*Topo Suicide*)-functionalized graphene device in the absence (a) and presence (b) of 300 pM hTop1 at 37 ± 1 °C in RB. The measured resistance of the device as a function of the applied gate voltage (V_{ecG}) and time (t), $R_{gr}(V_{ecG}, t)$ is plotted as a 2D map. In (b) the measurement starts in RB and the hTop1 containing solution is exchanged at around 10 min. The binding occurs for around 30 min, and subsequently the original RB is copiously exchanged. In (a) only the RB was exchanged at around 33 min. (c) Real-time profile of the Dirac point in the absence (black curve) and presence of 300 pM hTop1 (red curve) extracted from the 2D maps in (a) and (b) respectively. The gate voltage at which the graphene resistance is a maximum is extracted as the Dirac point at every cycle. The gray error bars indicate the error in the fit. The error bars are shown only for every second data point for clarity. The sudden jumps in the sensor response are due to solution exchange, during which time the measurement is paused. (d) Steady-state sensor response showing the gate dependence of graphene resistance ($R_{gr}(V_{ecG})$) at specific time instances (before, 9 min; during, 41 min; and after the addition of hTop1, 52 min in RB). There is a shift in the sensor response when going from RB (t = 9 min) to RB + hTop1 (t = 41 min). When coming back to RB (t = 52 min) there is no change signifying that hTop1 is still bound to the sensor surface.

of the thin electrical double layer at high ionic strength due to the presence of the carefully grafted polymer layer, which brings in an additional series capacitance as has been recently shown for organic transistors[57] and silicon nanowires.[58] We have previously demonstrated sensitivity at higher ionic strength using a similar strategy on CNTs[19] and graphene.[8]

It is now important to see if the enzyme is specifically bound and if the binding is covalent. In order to clarify this point, we have used a heat-inactivated form (HIPO) of the same hTop1 aliquot used above. Specifically, the protein solution is heated to 95 °C for 5 min and cooled down to room temperature before use. The enzyme loses its topoisomerase activity after this procedure, but it is still positively charged to undergo electrostatic interactions with the graphene-bound DNA. Support for this aspect is obtained from a relaxation assay comparing the active and heat-treated forms of hTop1 as presented in Figure S2. Figure 4 presents a representative example of the evolution of Dirac point during the interaction of HIPO with a DNA-functionalized graphene device followed by the response to active hTop1 on the same device. When going from the enzyme-containing solution to the RB, it is ensured that the washing is done thoroughly to remove any nonspecifically bound molecules. It is apparent from Figure 4 (black curve) that the Dirac point shifts down upon binding of HIPO, however, the initial response is recovered after the rigorous washing procedure, as expected for a nonspecifically bound protein. This suggests that any nonspecifically bound entities can be washed away. After exposure to 300 pM of active hTop1 it can be seen that the Dirac point shifts down persistently (red curve), confirming that we are indeed observing a specific covalent interaction of the active enzyme with the DNA attached to graphene. Further confirmation for this specific interaction is obtained by evaluating the sensor response in the absence of the capture DNA probe as shown in Figure S3. These observations strongly indicate that the active hTop1 is mostly covalently bound forming the cleavage complex, since otherwise it would have been washed away analogous to what happens in the case of HIPO. In order to completely assert the formation of a covalent bond, some spectroscopic information is necessary. However, we cannot obtain this information in

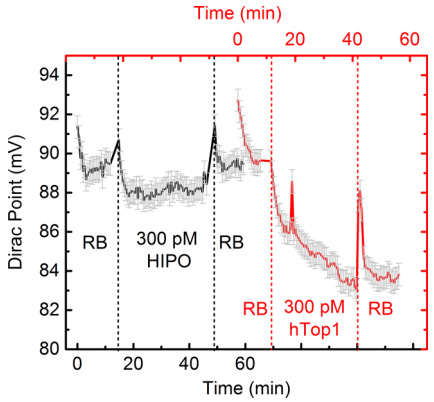

Figure 4. Specificity of the real-time sensor response. Sensor response (showing the real-time Dirac point profile, extracted from 2D maps measured at 37 ± 1 °C) to 300 pM each of a heat-inactivated form of hTop1 (HIPO, black curve) and of the active form of hTop1 (hTop1, red curve) measured consecutively on the same capture DNA (*Topo Suicide*)-functionalized graphene device. The measurement starts with a baseline in RB, followed by addition of the corresponding enzyme aliquot, after which the device is rinsed well before going back to the RB. For the inactive form, the initial response is recovered, while for the active form we see a persistent change in the Dirac point, which is attributed to the specific binding of the active form (see Figure S3 for a reference device without capture DNA probe). The peaks in the sensor response are due to solution exchange, while the peak in the middle of 300 pM hTop1 is due to some electrical noise.

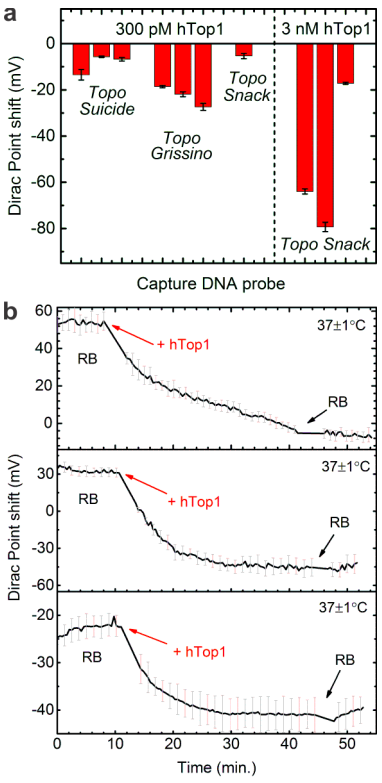

Figure 5. Steady-state and real-time sensor response to the different capture DNA probes. (a) Steady-state response. The shift in Dirac point (pH 7.5, 37 ± 1 °C) as a result of the cleavage reaction step is collected for many devices. This shift is calculated as the difference between the Dirac point in the initial RB to that in the final RB (after hTop1 binding and washing steps). It is apparent that in all cases, the Dirac point shifts to more negative values, with the response being stronger at higher concentrations. In the case of *Topo Snack* we have measured the sensor response mainly at 3 nM hTop1, since the shift was in most cases negligible at the lower concentration of 300 pM hTop1. (b) Real-time response to 3 nM of hTop1 for 3 representative devices modified with *Topo Snack*.

our scenario due to the small footprint of our sensor surface and the nonavailability of a clear spectroscopic fingerprint for the covalent bond formed during the cleavage reaction.

In order to evaluate the reproducibility and reliability of the sensing characteristics, we have measured the sensor response of different devices to three different capture DNA sequences shown in Figure 2: *Topo Suicide*, *Topo Snack*, and *Topo Grissino*. While all of them include the sequence (GACTT*AG) that is recognized by the hTop1 enzyme, there are only subtle differences in their composition (see SI for a discussion on the design rationale). Figure 5a presents the typical steady-state response of the three sets of devices to 300 pM hTop1 (and also to 3 nM hTop1 for the *Topo Snack* modified devices). The value of the Dirac point shift plotted here is the difference between the initial and final Dirac point in the RB, with the latter measured after the hTop1-binding and washing procedure. It is apparent that for all of the three cases, we can observe a consistent shift in the Dirac point toward negative values. Figure 5b shows the real-time response of three representative devices further confirming the Dirac point shift. The strength of the sensor response can be correlated with the fraction of the enzyme bound to DNA, which is different depending on the selected capture DNA.[59] This variation in probe-dependent sensor response strongly suggests that we are indeed observing a specific response. In addition to this, we indeed see device-to-device variations in the sensor response for a given capture DNA probe, which may be attributed to two aspects. The first one concerns the density of attached DNA molecules, which most likely varies from one device to the other due to local variations in chemical reactivity of CVD-graphene.[7,52,60] Second, the sensitivity is expected to vary from one device to another. Although we obtain low resistances in the order of 10 kΩ after the fabrication procedure, we observe variations in the field-effect characteristics from one device to the other, which is a common problem in CVD-grown graphene.[51]

Now we turn toward the concentration dependence of the kinetic response to the binding of hTop1. Since the binding of the enzyme to the substrate is covalent, it is not possible to reuse the same device for more than one concentration value, unless the response is weak for the lower concentrations. Due to this reason we have chosen the *Topo Snack* capture probe, which in general gives a weak or negligible sensor response for 300 pM hTop1. In this case, we can reuse the same

device and measure the response also at a higher concentration of 3 nM. Figure 6a presents such a measured data set, while the points in Figure 6b show the evolution of Dirac point for exposure to 300 pM hTop1 (black points) and 3 nM hTop1 (red points). (See Figure S4 for the steady-state response.) The solid lines in Figure 6b present a fit of the measured time response to a first-order 1:1 binding model (see SI for details of modeling).[61] From this analysis we extract a surface binding constant (K_D) value of 3.62 ± 0.27 nM for this device. The method for extracting K_D is presented in SI. For other devices modified with the *Topo Snack* probe, the K_D ranges from 1 to 4 nM, while for the *Topo Suicide*- and *Topo Grissino*-modified devices, we have extracted K_D in the range of 100−500 pM.

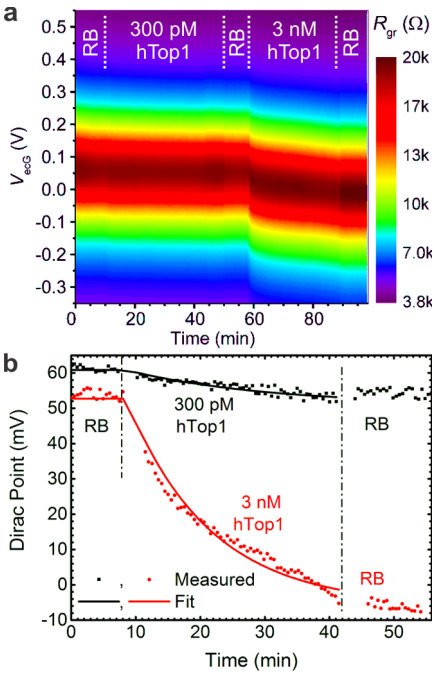

Figure 6. Binding kinetics of the hTop1 cleavage reaction. Real-time measurement of the concentration dependence of the sensor response to the binding of 300 pM (black curve) and 3 nM (red curve) of hTop1 on to capture DNA (*Topo Snack*)-modified graphene devices at pH7.5, 37 ± 1 °C. (a) 2D map showing $R_{gr}(V_{ecG}, t)$. (b) Measured (dots) and simulated (lines) real-time kinetic profiles for the binding of hTop1 on to the capture DNA immobilized on graphene. The fitting was done by assuming a first-order binding model, which gives a surface binding constant of 3.62 ± 0.27 nM for this device.

Finally, we turn toward the observation of the complete catalytic cycle, where both the hTop1 catalytic steps mentioned in Figure 2 were carried out. Figure 7a shows a representative curve where the cleavage reaction was measured by addition of hTop1 on to DNA-functionalized graphene, followed by washing and subsequent addition of the religation DNA strand (final concentration of 1 μM). The cleavage reaction was monitored for 30 min, while the religation reaction was monitored in this case for 40 min. It is apparent that the binding of hTop1 can be confirmed by the negative shift in Dirac point as discussed in the previous cases. However, with the addition of the religation strand, we can recover only part of the initial response. We have observed such a response in many of the measured samples even for longer time periods. We attribute the incomplete recovery of the original response to the fact that hTop1 remains permanently bound (within the time scale of the experiment) on to the DNA probe. There may be several reasons for this including the use of a heterogeneous format (electrostatic/hydrophobic interactions between the chip surface and the biomolecules, which do not occur in homogeneous relaxation assays) and the additional charge due to the religation strand. We gather support for this behavior by observing that the noise in the sensor response (t > 60 min) is found to be much higher in the presence of the religation strand. This is further attested by the AFM images (Figures 7b,c and S5) taken after the measurement cycle showing the presence of some spots on the graphene surface, which are attributed to the leftover enzyme molecules.

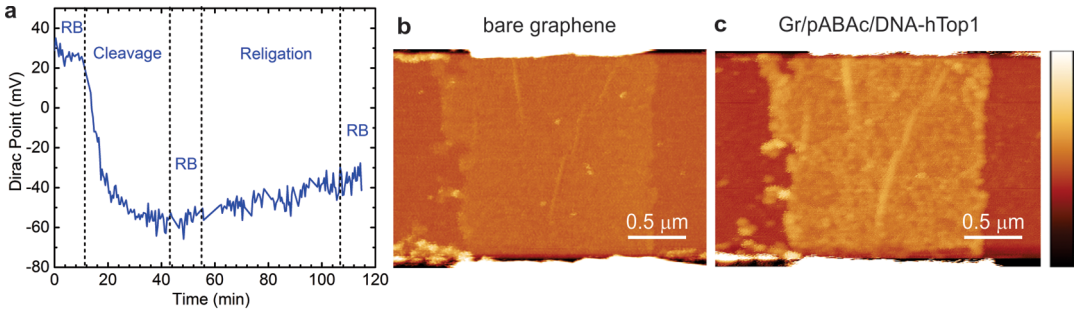

Figure 7. Real-time detection of the complete hTop1 catalytic cycle. (a) Real-time evolution of the Dirac point of a capture DNA (*Topo Snack*)-functionalized graphene device during the cleavage and religation reaction steps (pH 7.5, 37 ± 1 °C). After measuring the baseline in RB, hTop1 is introduced into the microwell, and the binding occurs for around 30 min. This is followed by washing and measurement in RB (at around 43 min). Subsequently the religation oligonucleotide was added in steps (starting at around 58 min up to a final concentration of 1 μM), and the response monitored for 40 min. Finally the RB was exchanged at 110 min. (b,c) AFM images of the device before (b) and (c) after the sensor trials. In (c) it is apparent that the surface is rough with many spots (see line profiles in Figure S3), which we attribute to remaining enzyme molecules after the sensor trial. The height scale bar is 38 nm in both cases.

The rather irreversible nature of the sensor response suggests that we may be able to deploy such graphene sensors for the screening of class I drugs, targeting mainly the cleavage reaction step as discussed earlier. This motivates the future application of our graphene sensors as diagnostic tools for the detection of topoisomerase I cleavage activity from microorganisms such as malaria-causing *Plasmodium* parasites, where the use of other techniques such as rolling circle amplification still poses several problems.[62] In order to correlate the efficacy of a selected drug with the sensor response, the sensor trials will be carried out without and with the drug. In the presence of an effective drug, we expect to see a different kinetic response (*e.g.*, a smaller binding constant), while with an ineffective drug the kinetic parameters will remain largely unaffected.

CONCLUSIONS

In conclusion, we have demonstrated a graphene strip field-effect sensor for real-time observation of binding kinetics of enzyme–substrate interactions. Specifically, we have detected the activity of a topoisomerase (hTop1) by immobilizing its substrate (DNA) as a capture probe on to graphene. In addition to being able to estimate the binding constant of the enzyme to its substrate we have shown that the catalytic reaction can be followed giving us real-time information about the various interactions. Specifically, we were successful in the decoupled observation of the cleavage reaction step of topoisomerase activity down to picomolar enzyme concentrations. The presented results show promise for using liquid-gated graphene sensors as an electronic alternative for assessing binding kinetics of other enzyme–substrate interactions as well as in general for the study of binding kinetics. Moreover, the capability to estimate topoisomerase activity using a simple and straightforward protocol will allow for its use as a rapid screening platform for screening the efficacy of anticancer drugs.

METHODS

Enzyme Preparation. The purification of hTop1 proteins was carried out essentially as previously described.[43] Briefly, hTop1 was expressed in the *Saccharomyces cerevisiae* strain EKY3 (ura3−52, his3Δ200, leu2Δ1, trp1Δ63, hTop1::TRP1, MATα), which lacks the endogenous hTop1 (EKY3-ΔTop1). The YCp-GAL1-e-hTop1 single copy plasmid, containing the hTop1 gene, was transformed in EKY3-ΔTop1 yeast cells for the expression of hTop1.[63] The transformed cells were selected on URA$^-$ dextrose, since YCpGAL1-e-hTop1 contains the allele ura3−52, which confers them the capacity to grow in the absence of uracil. Few (2−3) transformed colonies were scraped from URA$^-$ 2% dextrose plate and transferred to fresh liquid URA$^-$ dextrose. Since the hTop1 gene transcription is under the control of GAL1 promoter, the cells were diluted in URA$^-$ 2% raffinose to enable the cells to consume all the glucose, and at A590 = 0.8−2% galactose was added to induce the synthesis of hTop1. EKY3 cells were disrupted by mechanical lysis. For the purification of hTop1 from the cellular extract, the ANTI-FLAG M2 affinity gel (Sigma-Aldrich) was used. ANTI-FLAG M2 is a purified murine IgG1 monoclonal antibody covalently attached to agarose, able to bind the FLAG fusion proteins, such as our recombinant hTop1. The cellular extract was loaded onto the column under gravity flux. The elution of hTop1 was obtained by competition with the FLAG peptide (Sigma-Aldrich). Sequential aliquots of 500 μL of eluted protein were collected, adding to each aliquot 500 μL of 80% glycerol supplemented with proteases inhibitors. Next, the hTop1 aliquots were separated according to molecular weight on a denaturing polyacrylamide gel. After the separation in the gel, the proteins were transferred onto a nitrocellulose membrane. The proteins were detected using two different antibodies: the mouse monoclonal ANTI-FLAG M2-alkaline phosphatase antibody (used to verify the absence of enzyme degradation) and the Anti-Topoisomerase I antibody (used to quantify the amount of enzyme in the aliquots). For the ANTI-FLAG M2-alkaline phosphatase antibody (Sigma-Aldrich), the membrane was exposed to the substrate of alkaline phosphatase (BCIP/NT) to visualize the protein band. For the Anti-Topoisomerase I antibody (Abcam-ab58313), the secondary antibody (Abcam-ab97240) was conjugated to Horseradish peroxidase (HRP), which is detectable by enhanced chemiluminescence (ECL). We used ImageJ software to calculate the concentrations of hTop1 aliquots by densitometry using as reference the hTop1, with a defined concentration, purchased from TopoGEN.[43]

Graphene Devices. Ti/Pt electrodes lines were prepatterned using photolithography on a silicon wafer with insulating oxide (500 nm) on both sides. The wafer was spin-coated with a protective resist and diced into individual chips. The chips are 3 cm long and 0.5 cm wide and incorporate six platinum electrode pairs each separated by a gap of approximately 4 μm. CVD-grown graphene was procured commercially (Graphene Supermarket Inc.) or obtained by a "peel-off" strategy.[51] The graphene-on-copper foils (2 × 2 in and 20 μm thick) were cut into pieces of around 1 × 0.5 cm. The transfer was done either using poly(methyl methacrylate) (PMMA) or poly(styrene) (PS). The polymer was first spin-coated on one side and dried at 75 °C for 10 min. The underlying copper layer was removed by etching in an aqueous solution of 0.4 M H_2O_2 and 2 M HCl. Then, graphene was transferred to Si/SiO_2 chips with the prepatterned Ti/Pt electrode lines and baked in the oven at 95 °C for 20 min before removal of PS or PMMA using toluene or *N*-(m)ethylpyrrolidone, respectively. The patterning of the flakes was also performed by photolithography. For this purpose, 10 nm of copper was first evaporated on graphene to be used as a sacrificial protective layer in order that the photoresist does not come in direct contact with the graphene surface. Following this, the structures are patterned using a positive process using the resist S1805 (Microposit). After exposure and development the unprotected regions are removed using mild oxygen plasma etching. After this, the resist and the remaining copper are removed in *N*-ethylpyrrolidone and HCl/H_2O_2, respectively. Subsequently we do another round of lithography to deposit silicon oxide by thermal evaporation in order to passivate all electrode lines using an insulating layer. This ensures that graphene is exclusively in contact with the solution. The chips were then annealed at 585 °C for 60 s in argon atmosphere to remove organic impurities and to improve the contact between graphene and the electrodes/chip. In some samples, a mild piranha etch (<5 s) was necessary to remove organic contaminants completely (as inferred from AFM images). Finally, an electrochemical etching procedure was carried out in HCl in order to remove trace metal impurities present on patterned graphene.[64]

Electrical Measurements. For the measurements in the liquid gated configuration,[10,19] the samples were fixed on a chip carrier, and the electrodes were bonded using a manual chip bonder. A PDMS plate was cut, shaped as a channel connecting

two reservoirs, and placed above the gaps between the electrodes. The chip carrier holding the sample was then connected to the Agilent E-4980A LCR meter. The measurements were recorded for a single electrode pair, referred to as device. Usually, the device was operated at 1 kHz and 10−20 mV bias. The gate voltage was applied using an Ag/AgCl reference electrode (WPI Inc.), immersed in the liquid. 0 mV vs Ag/AgCl corresponds to 50 ± 5 mV vs SCE measured in 0.1 M KCl. The gate voltage is continuously swept in a fixed range, and the real part of the impedance recorded to obtain the sensor responses. The response of the sensor was recorded as a 2D map containing the variation of the resistance as a function of gate voltage and measurement cycle. When exchanging from one liquid to the other, the measurement is stopped at a gate voltage of 0 V. As a result, the cycle number increments by one when going from one solution to other, however there is a time delay introduced during the solution exchange. Since we need an equal spacing for plotting the 2D maps, there is a slight mismatch (<3 min) between the actual timing and the timing in the 2D maps. The experiments were carried out in a total of 21 different devices: 7 devices using *Topo Suicide*, 9 devices using *Topo Grissino*, and 5 devices using *Topo Snack* substrates.

Electrochemical Modification and DNA Coupling. The electrochemical modification was carried out via an oxidative polymerization.[8] A PDMS channel was filled up with the solution containing the monomeric precursor. An Ag/AgCl electrode was used as reference electrode. The setup used was the same as mentioned for the electrical measurements. For the modification of graphene strips with carboxylic groups, a solution of ethanol containing 10 mM 4-aminobenzoic acid (ABAc) and 100 mM $LiClO_4$ was loaded into the channel. The voltage at graphene was swept from −0.3 to +0.9 V against the Ag/AgCl electrode for 8 cycles. Following this, the coupling of the amino-terminated capture DNA sequences (Figure 2d−f) was carried out.[19] The capture DNA oligos were obtained from Eurofins MWG Operon, except for AG which was procured from Gene Link Inc. The ethylenediaminechloride/*N*-hydroxysuccinimide (EDC/NHS) activation of the carboxylic groups was performed at room temperature. The reaction was completed in 15 min, using a mixture of 0.2 M EDC and 0.1 M NHS freshly prepared in 10 mM potassium phosphate buffer pH 6. The DNA coupling reaction was also carried out at room temperature, using 100 nM of capture DNA probe in 10 mM potassium phosphate buffer pH 7.4. Residual activated carboxylic groups were blocked using 20 mM ethanolamine. During the entire coupling procedure and the subsequent trials, the chip is maintained continuously in an aqueous environment without drying at any time. To remove nonspecifically bound entities, a rigorous washing procedure was used.

Conflict of Interest: The authors declare no competing financial interest.

Supporting Information Available: The Supporting Information is available free of charge on the ACS Publications website at DOI: 10.1021/acsnano.5b05709.

Terminology used, details about the attachment of DNA on to graphene, details about the choice of DNA sequences, comparison of active hTop1 and its heat-treated form (HIPO), hTop1 response in a reference device without capture DNA probe, the binding model for extracting K_D, the concentration dependence of the equilibrium sensor response (gate dependence curves), the line profiles from AFM images, and specificity of the sensor response (PDF)

Acknowledgment. We are grateful to Alec Wodtke (Max Planck Institute for Biophysical Chemistry, Göttingen) for graphene samples. We thank Yvonne Link and Stephan Schmid for help with metal deposition. We thank Janina Krieg for the preparation of layout images. Cinzia Tesauro acknowledges a Post-Doc fellowship from the Carlsberg Foundation.

REFERENCES AND NOTES

1. Balasubramanian, K.; Kern, K. 25th Anniversary Article: Label-Free Electrical Biodetection Using Carbon Nanostructures. *Adv. Mater.* **2014**, *26*, 1154–1175.
2. Liu, Y. X.; Dong, X. C.; Chen, P. Biological and Chemical Sensors Based on Graphene Materials. *Chem. Soc. Rev.* **2012**, *41*, 2283–2307.
3. Schedin, F.; Geim, A. K.; Morozov, S. V.; Hill, E. W.; Blake, P.; Katsnelson, M. I.; Novoselov, K. S. Detection of Individual Gas Molecules Adsorbed on Graphene. *Nat. Mater.* **2007**, *6*, 652–655.
4. Georgakilas, V.; Otyepka, M.; Bourlinos, A. B.; Chandra, V.; Kim, N.; Kemp, K. C.; Hobza, P.; Zboril, R.; Kim, K. S. Functionalization of Graphene: Covalent and Non-Covalent Approaches, Derivatives and Applications. *Chem. Rev.* **2012**, *112*, 6156–6214.
5. Liu, J. Q.; Liu, Z.; Barrow, C. J.; Yang, W. R. Molecularly Engineered Graphene Surfaces for Sensing Applications: A Review. *Anal. Chim. Acta* **2015**, *859*, 1–19.
6. Sundaram, R. S.; Gomez-Navarro, C.; Balasubramanian, K.; Burghard, M.; Kern, K. Electrochemical Modification of Graphene. *Adv. Mater.* **2008**, *20*, 3050–3053.
7. Balasubramanian, K.; Zuccaro, L.; Kern, K. Tunable Enhancement of Raman Scattering in Graphene-Nanoparticle Hybrids. *Adv. Funct. Mater.* **2014**, *24*, 6348–6358.
8. Zuccaro, L.; Krieg, J.; Desideri, A.; Kern, K.; Balasubramanian, K. Tuning the Isoelectric Point of Graphene by Electrochemical Functionalization. *Sci. Rep.* **2015**, *5*, 11794.
9. Patil, A. V.; Fernandes, F. B.; Bueno, P. R.; Davis, J. J. Graphene-Based Protein Biomarker Detection. *Bioanalysis* **2015**, *7*, 725–742.
10. Kurkina, T.; Sundaram, S.; Sundaram, R. S.; Re, F.; Masserini, M.; Kern, K.; Balasubramanian, K. Self-Assembled Electrical Biodetector Based on Reduced Graphene Oxide. *ACS Nano* **2012**, *6*, 5514–5520.
11. Green, N. S.; Norton, M. L. Interactions of DNA with Graphene and Sensing Applications of Graphene Field-Effect Transistor Devices: A Review. *Anal. Chim. Acta* **2015**, *853*, 127–142.
12. Stine, R.; Mulvaney, S. P.; Robinson, J. T.; Tamanaha, C. R.; Sheehan, P. E. Fabrication, Optimization, and Use of Graphene Field Effect Sensors. *Anal. Chem.* **2013**, *85*, 509–521.
13. Zhan, B. B.; Li, C.; Yang, J.; Jenkins, G.; Huang, W.; Dong, X. C. Graphene Field-Effect Transistor and Its Application for Electronic Sensing. *Small* **2014**, *10*, 4042–4065.
14. Yan, F.; Zhang, M.; Li, J. H. Solution-Gated Graphene Transistors for Chemical and Biological Sensors. *Adv. Healthcare Mater.* **2014**, *3*, 313–331.
15. Schaasfoort, R. B.; Tudos, A. J. *Handbook of Surface Plasmon Resonance*; RSC Publishing: Cambridge, 2008.
16. Hill, R. T. Plasmonic Biosensors. *Wiley Interdisciplinary Reviews-Nanomedicine and Nanobiotechnology* **2015**, *7*, 152–168.
17. Vollmer, F.; Yang, L. Label-Free Detection with High-Q Microcavities: A Review of Biosensing Mechanisms for Integrated Devices. *Nanophotonics* **2012**, *1*, 267–291.
18. Waggoner, P. S.; Craighead, H. G. Micro- and Nanomechanical Sensors for Environmental, Chemical, and Biological Detection. *Lab Chip* **2007**, *7*, 1238–1255.
19. Kurkina, T.; Vlandas, A.; Ahmad, A.; Kern, K.; Balasubramanian, K. Label-Free Detection of Few Copies of DNA with Carbon Nanotube Impedance Biosensors. *Angew. Chem., Int. Ed.* **2011**, *50*, 3710–3714.
20. Bunimovich, Y. L.; Shin, Y. S.; Yeo, W. S.; Amori, M.; Kwong, G.; Heath, J. R. Quantitative Real-Time Measurements of DNA Hybridization with Alkylated Nonoxidized Silicon Nanowires in Electrolyte Solution. *J. Am. Chem. Soc.* **2006**, *128*, 16323–16331.
21. Duan, X. X.; Li, Y.; Rajan, N. K.; Routenberg, D. A.; Modis, Y.; Reed, M. A. Quantification of the Affinities and Kinetics of Protein Interactions Using Silicon Nanowire Biosensors. *Nat. Nanotechnol.* **2012**, *7*, 401–407.
22. De, A.; van Nieuwkasteele, J.; Carlen, E. T.; van den Berg, A. In Real-Time Measurements of Pna:DNA Hybridization Kinetics with Silicon Nanowire Biosensors. 2013 Transducers & Eurosensors XXVII: The 17th International Conference on Solid-State Sensors, Actuators and Microsystems (TRANSDUCERS & EUROSENSORS XXVII), Barcelona, Spain, June 16−20, 2013; IEEE: New York, **2013**; pp 2795−2798.

23. Stine, R.; Robinson, J. T.; Sheehan, P. E.; Tamanaha, C. R. Real-Time DNA Detection Using Reduced Graphene Oxide Field Effect Transistors. *Adv. Mater.* **2010**, *22*, 5297–5300.
24. Yin, Z. Y.; He, Q. Y.; Huang, X.; Zhang, J.; Wu, S. X.; Chen, P.; Lu, G.; Chen, P.; Zhang, Q. C.; Yan, Q. Y.; et al. Real-Time DNA Detection Using Pt Nanoparticle-Decorated Reduced Graphene Oxide Field-Effect Transistors. *Nanoscale* **2012**, *4*, 293–297.
25. Mu, L. Y.; Droujinine, I. A.; Rajan, N. K.; Sawtelle, S. D.; Reed, M. A. Direct, Rapid, and Label-Free Detection of Enzyme Substrate Interactions in Physiological Buffers Using Cmos-Compatible Nanoribbon Sensors. *Nano Lett.* **2014**, *14*, 5315–5322.
26. Choi, Y. K.; Moody, I. S.; Sims, P. C.; Hunt, S. R.; Corso, B. L.; Perez, I.; Weiss, G. A.; Collins, P. G. Single-Molecule Lysozyme Dynamics Monitored by an Electronic Circuit. *Science* **2012**, *335*, 319–324.
27. Olsen, T. J.; Choi, Y.; Sims, P. C.; Gu, O. T.; Corso, B. L.; Dong, C. J.; Brown, W. A.; Collins, P. G.; Weiss, G. A. Electronic Measurements of Single-Molecule Processing by DNA Polymerase I (Klenow Fragment). *J. Am. Chem. Soc.* **2013**, *135*, 7855–7860.
28. Sims, P. C.; Moody, I. S.; Choi, Y.; Dong, C. J.; Iftikhar, M.; Corso, B. L.; Gul, Q. T.; Collins, P. G.; Weiss, G. A. Electronic Measurements of Single-Molecule Catalysis by Camp-Dependent Protein Kinase A. *J. Am. Chem. Soc.* **2013**, *135*, 7861–7868.
29. Champoux, J. J. DNA Topoisomerases: Structure, Function, and Mechanism. *Annu. Rev. Biochem.* **2001**, *70*, 369–413.
30. Chen, S. H.; Chan, N. L.; Hsieh, T. S. New Mechanistic and Functional Insights into DNA Topoisomerases. *Annu. Rev. Biochem.* **2013**, *82*, 139–170.
31. Redinbo, M. R.; Stewart, L.; Champoux, J. J.; Hol, W. G. J. Structural Flexibility in Human Topoisomerase I Revealed in Multiple Non-Isomorphous Crystal Structures. *J. Mol. Biol.* **1999**, *292*, 685–696.
32. Stewart, L.; Redinbo, M. R.; Qiu, X. Y.; Hol, W. G. J.; Champoux, J. J. A Model for the Mechanism of Human Topoisomerase I. *Science* **1998**, *279*, 1534–1541.
33. Pommier, Y. Topoisomerase I Inhibitors: Camptothecins and Beyond. *Nat. Rev. Cancer* **2006**, *6*, 789–802.
34. Pommier, Y. DNA Topoisomerase I Inhibitors: Chemistry, Biology, and Interfacial Inhibition. *Chem. Rev.* **2009**, *109*, 2894–2902.
35. Pommier, Y.; Pourquier, P.; Urasaki, Y.; Wu, J. X.; Laco, G. S. Topoisomerase I Inhibitors: Selectivity and Cellular Resistance. *Drug Resist. Updates* **1999**, *2*, 307–318.
36. Fiorani, P.; Bruselles, A.; Falconi, M.; Chillemi, G.; Desideri, A.; Benedetti, P. Single Mutation in the Linker Domain Confers Protein Flexibility and Camptothecin Resistance to Human Topoisomerase I. *J. Biol. Chem.* **2003**, *278*, 43268–43275.
37. D'Annessa, I.; Tesauro, C.; Wang, Z. X.; Arno, B.; Zuccaro, L.; Fiorani, P.; Desideri, A. The Human Topoisomerase 1b Arg634ala Mutation Results in Camptothecin Resistance and Loss of Inter-Domain Motion Correlation. *Biochim. Biophys. Acta, Proteins Proteomics* **2013**, *1834*, 2712–2721.
38. Nitiss, J. L.; Soans, E.; Rogojina, A.; Seth, A.; Mishina, M. Topoisomerase Assays. *Current Protocols in Pharmacology*, 2012; Supplement 57, Unit 3.3.
39. Castelli, S.; Coletta, A.; D'Annessa, I.; Fiorani, P.; Tesauro, C.; Desideri, A. Interaction between Natural Compounds and Human Topoisomerase I. *Biol. Chem.* **2012**, *393*, 1327–40.
40. Yang, Z.; Champoux, J. J. Reconstitution of Enzymatic Activity by the Association of the Cap and Catalytic Domains of Human Topoisomerase I. *J. Biol. Chem.* **2002**, *277*, 30815–23.
41. Christiansen, K.; Svejstrup, A. B. D.; Andersen, A. H.; Westergaard, O. Eukaryotic Topoisomerase I-Mediated Cleavage Requires Bipartite DNA Interaction - Cleavage of DNA Substrates Containing Strand Interruptions Implicates a Role for Topoisomerase-I in Illegitimate Recombination. *J. Biol. Chem.* **1993**, *268*, 9690–9701.
42. Jepsen, M. L.; Ottaviani, A.; Knudsen, B. R.; Ho, Y. P. Quantum Dot Based DNA Nanosensors for Amplification-Free Detection of Human Topoisomerase I. *RSC Adv.* **2014**, *4*, 2491–2494.
43. Zuccaro, L.; Tesauro, C.; Cerroni, B.; Ottaviani, A.; Knudsen, B. R.; Balasubramanian, K.; Desideri, A. Rolling Circle Amplification-Based Detection of Human Topoisomerase I Activity on Magnetic Beads. *Anal. Biochem.* **2014**, *451*, 42–44.
44. Dezhenkova, L. G.; Tsvetkov, V. B.; Shtil, A. A. Topoisomerase I and Ii Inhibitors: Chemical Structure, Mechanisms of Action and Role in Cancer Chemotherapy. *Russ. Chem. Rev.* **2014**, *83*, 82–94.
45. Marcussen, L. B.; Jepsen, M. L.; Kristoffersen, E. L.; Franch, O.; Proszek, J.; Ho, Y. P.; Stougaard, M.; Knudsen, B. R. DNA-Based Sensor for Real-Time Measurement of the Enzymatic Activity of Human Topoisomerase I. *Sensors* **2013**, *13*, 4017–4028.
46. Kristoffersen, E. L.; Jorgensen, L. A.; Franch, O.; Etzerodt, M.; Frohlich, R.; Bjergbaek, L.; Stougaard, M.; Ho, Y. P.; Knudsen, B. R. Real-Time Investigation of Human Topoisomerase I Reaction Kinetics Using an Optical Sensor: A Fast Method for Drug Screening and Determination of Active Enzyme Concentrations. *Nanoscale* **2015**, *7*, 9825–9834.
47. Tsai, H. P.; Lin, L. W.; Lai, Z. Y.; Wu, J. Y.; Chen, C. E.; Hwang, J.; Chen, C. S.; Lin, C. M. Immobilizing Topoisomerase I on a Surface Plasmon Resonance Biosensor Chip to Screen for Inhibitors. *J. Biomed. Sci.* **2010**, *17*, 49.
48. Tiwari, P. B.; Annamalai, T.; Cheng, B. K.; Narula, G.; Wang, X. W.; Tse-Dinh, Y. C.; He, J.; Darici, Y. A Surface Plasmon Resonance Study of the Intermolecular Interaction between Escherichia Coli Topoisomerase I and Pbad/Thio Supercoiled Plasmid DNA. *Biochem. Biophys. Res. Commun.* **2014**, *445*, 445–450.
49. Pond, C. D.; Holden, J. A.; Schnabel, P. C.; Barrows, L. R. Surface Plasmon Resonance Analysis of Topoisomerase I-DNA Binding: Effect of Mg2+ and DNA Sequence. *Anti-Cancer Drugs* **1997**, *8*, 336–344.
50. Sikder, D.; Unniraman, S.; Bhaduri, T.; Nagaraja, V. Functional Cooperation between Topoisomerase I and Single Strand DNA-Binding Protein. *J. Mol. Biol.* **2001**, *306*, 669–679.
51. Yu, H. K.; Balasubramanian, K.; Kim, K.; Lee, J. L.; Maiti, M.; Ropers, C.; Krieg, J.; Kern, K.; Wodtke, A. M. Chemical Vapor Deposition of Graphene on a "Peeled-Off" Epitaxial Cu(111) Foil: A Simple Approach to Improved Properties. *ACS Nano* **2014**, *8*, 8636–8643.
52. Zuccaro, L.; Kern, K.; Balasubramanian, K. Identifying Chemical Functionalization on Individual Carbon Nanotubes and Graphene by Local Vibrational Fingerprinting. *ACS Nano* **2015**, *9*, 3314–3323.
53. Beretta, G. L.; Gatti, L.; Perego, P.; Zaffaroni, N. Camptothecin Resistance in Cancer: Insights into the Molecular Mechanisms of a DNA-Damaging Drug. *Curr. Med. Chem.* **2013**, *20*, 1541–1565.
54. Andersen, A. H.; Gocke, E.; Bonven, B. J.; Nielsen, O. F.; Westergaard, O. Topoisomerase-I Has a Strong Binding Preference for a Conserved Hexadecameric Sequence in the Promotor Region of the Ribosomal-Rna Gene from Tetrahymena-Pyriformis. *Nucleic Acids Res.* **1985**, *13*, 1543–1557.
55. Christiansen, K.; Westergaard, O. Characterization of Intramolecular and Intermolecular DNA Ligation-Mediated by Eukaryotic Topoisomerase-I - Role of Bipartite DNA Interaction in the Ligation Process. *J. Biol. Chem.* **1994**, *269*, 721–729.
56. Balasubramanian, K.; Kurkina, T.; Ahmad, A.; Burghard, M.; Kern, K. Tuning the Functional Interface of Carbon Nanotubes by Electrochemistry: Toward Nanoscale Chemical Sensors and Biosensors. *J. Mater. Res.* **2012**, *27*, 391–402.
57. Palazzo, G.; De Tullio, D.; Magliulo, M.; Mallardi, A.; Intranuovo, F.; Mulla, M. Y.; Favia, P.; Vikholm-Lundin, I.; Torsi, L. Detection Beyond Debye's Length with an Electrolyte-Gated Organic Field-Effect Transistor. *Adv. Mater.* **2015**, *27*, 911–916.
58. Gao, N.; Zhou, W.; Jiang, X. C.; Hong, G. S.; Fu, T. M.; Lieber, C. M. General Strategy for Biodetection in High Ionic

Strength Solutions Using Transistor-Based Nanoelectronic Sensors. *Nano Lett.* **2015**, *15*, 2143–2148.
59. Renodon-Corniere, A.; Jensen, L. H.; Nitiss, J. L.; Jensen, P. B.; Sehested, M. Interaction of Human DNA Topoisomerase Ii Alpha with DNA: Quantification by Surface Plasmon Resonance. *Biochemistry* **2002**, *41*, 13395–13402.
60. Guell, A. G.; Ebejer, N.; Snowden, M. E.; Macpherson, J. V.; Unwin, P. R. Structural Correlations in Heterogeneous Electron Transfer at Monolayer and Multilayer Graphene Electrodes. *J. Am. Chem. Soc.* **2012**, *134*, 7258–7261.
61. Oshannessy, D. J.; Brighamburke, M.; Soneson, K. K.; Hensley, P.; Brooks, I. Determination of Rate and Equilibrium Binding Constants for Macromolecular Interactions Using Surface-Plasmon Resonance - Use of Nonlinear Least-Squares Analysis-Methods. *Anal. Biochem.* **1993**, *212*, 457–468.
62. Juul, S.; Nielsen, C. J. F.; Labouriau, R.; Roy, A.; Tesauro, C.; Jensen, P. W.; Harmsen, C.; Kristoffersen, E. L.; Chiu, Y. L.; Frohlich, R.; et al. Droplet Microfluidics Platform for Highly Sensitive and Quantitative Detection of Malaria-Causing Plasmodium Parasites Based on Enzyme Activity Measurement. *ACS Nano* **2012**, *6*, 10676–10683.
63. Bjornsti, M. A.; Benedetti, P.; Viglianti, G. A.; Wang, J. C. Expression of Human DNA Topoisomerase-I in Yeast-Cells Lacking Yeast DNA Topoisomerase-I - Restoration of Sensitivity of the Cells to the Antitumor Drug Camptothecin. *Cancer Res.* **1989**, *49*, 6318–6323.
64. Iost, R. M.; Crespilho, F. N.; Zuccaro, L.; Yu, H. K.; Wodtke, A. M.; Kern, K.; Balasubramanian, K. Enhancing the Electrochemical and Electronic Performance of Cvd-Grown Graphene by Minimizing Trace Metal Impurities. *ChemElectroChem* **2014**, *1*, 2070–2074.